Learning Robot Motion in a Cluttered Environment Using Unreliable Human Skeleton Data Collected by a Single RGB Camera

Ryota Takamido and Jun Ota, *Member, IEEE*

***Abstract*—Existing learning from demonstration (LfD) frameworks have difficulty dealing with unreliable and limited number of demonstrations. To address this issue, we proposed a new motion planning framework named experience-driven random tree connect with human demonstration (ERTC-HD), which can facilitate the identification of valid motions in cluttered environments by only using human skeleton information extracted from a single red, green, and blue (RGB) camera. The concept of this framework is to only extract the comprehensive features of human motion from unreliable demonstrations and use it as a rough clue for solving difficult planning problems instead of as a strict solution. During the process of ERTC-HD, robot motions generated from extracted comprehensive features of human motion are saved as a path experience and modified through the path adaptation process of the existing ERTC planner when transferring it to the new problem. The results of three simulation experiments revealed that the ERTC-HD could identify valid motion in cluttered environments within a shorter time than other state-of-the-art planners, even when using unreliable demonstration data collected by a single RGB camera. Reducing the required accuracy of the original information resources can extend the range of LfD framework applications.**

***Index Terms*—Cluttered environment, experience-based motion planning, learning from demonstration, human skeleton.**

I. Introduction

THE concept of learning from human demonstration (LfD), in which robots learn new skills and motions from human demonstration, has achieved significant success in robot motion planning [1]. In this regard, the recent advances in image processing technology, such as the development of skeletal tracking techniques using a single red, green, and blue (RGB) camera, make collecting human motion data easier [2]. While existing learning techniques, such as kinesthetic learning, require expertise for robot manipulation [3], human demonstrators can teach new motions by demonstrating in front of the camera the ideal motions with their own body; hence, learning with human demonstrators is more intuitive and user-friendly for non-expert users.

However, this approach has only been applied to simple planning problems owing to certain unsolved issues [4], [5], [6], [7], [8]. The first one is generating valid, collision-free robot motion using unreliable demonstrations. Because the accuracy of demonstrations obtained from such a simple measurement system tends to be poor due to the estimation error of the human skeleton [9], applying LfD methodologies that aim for precise reproduction of "human-like motion" [10] leads to collisions with obstacles when a robot moves in cluttered environments.

The second problem is generalizing the limited number of unreliable demonstrations. Since it is difficult to obtain many demonstrations from human demonstrators, a limited number of demonstrations should be generalized to different environments and tasks. The generalizability of demonstration data is a well-known problem; however, if noisy and small-sized data are directly learned and generalized, the generalization error increases [11].

To address these two challenges, this study proposes a new LfD framework that can facilitate difficult motion planning in a cluttered environment, such as planning for picking up a closely lined-up object from a shelf by only using an unreliable human skeleton data collected via a single RGB camera.

II. Related Work

A. LFD Studies in Robot Motion Planning

There are numerous existing LfD studies in the robot motion planning field [1]. Among them, using skeleton information extracted from image data collected via a single vision sensor is the easiest compared to conventional data collection techniques such as kinesthetic teaching [12]. Therefore, several recent studies have attempted to use image data collected by a single vision sensor to solve planning problems such as writing characters [7], carrying objects [4], [5], object manipulation [8], and tracking pedestrians [6]. However, these methods can only be applied in less cluttered environments with few obstacles [4], [5], [6], [7], or they require additional information such as the 3D model of objects [8]. Therefore, as of now, obstacle-avoidant motion has not been successfully generated using such a simple measurement system in a cluttered environment.

Theoretically, the methods in existing LfD studies can be roughly divided into learning-based and model-based approaches. The former uses a machine learning technique to learn the feature and policy of human demonstration. Among them, reinforcement learning (RL) and inverse RL (IRL) have

Manuscript received 8 April 2023; accepted 9 July 2023. Date of publication 19 July 2023; date of current version 25 July 2023. This letter was recommended for publication by Associate Editor S. Bansal and Editor A. Faust upon evaluation of the reviewers' comments. This work was supported by New Energy and Industrial Technology Development Organization (NEDO) under Project JPNP20016. *(Corresponding author: Ryota Takamido.)*

The authors are with the Research into Artifacts, Center for Engineering (RACE), School of Engineering, The University of Tokyo, Tokyo 113-0033, Japan (e-mail: takamido@race.t.u-tokyo.ac.jp; ota@race.t.u-tokyo.ac.jp).

This letter has supplementary downloadable material available at https://doi.org/10.1109/LRA.2023.3296930, provided by the authors.

Digital Object Identifier 10.1109/LRA.2023.3296930

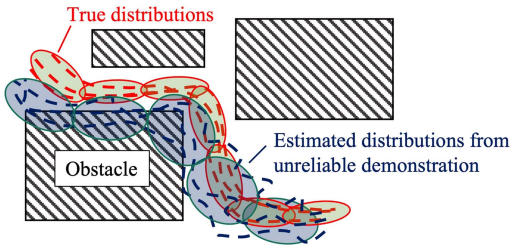

Fig. 1. Effect of unreliability of demonstration data on stochastic modeling.

demonstrated considerable success in planning fields owing to their high generalizability of demonstration data to different environments and tasks [13], [14] and studies that used RGB image data as information resources are especially related to this study [15], [16], [17]. However, this approach requires a large number of reliable training data [3]. Although some studies performed RL through off-line simulations, which enabled the collection of a large amount of data, such as in [14], the training time will increase when the planning problem is more complicated. Moreover, non-expert users find setting proper cost functions or hyper parameters for RL difficult. Hence, it is challenging to apply RL to the subject of this study.

A model-based approach can construct a mathematical model for representing demonstration data and generalize it to the new problem by tuning model parameters. Among them, stochastic models such as Gaussian mixture regression (GMR) or Gaussian mixture model (GMR) are frequently adopted in LfD studies [18], [19], [20]. In these studies, adding the bias to the sampling region of a motion planner based on generated distributions from demonstrations can ensure reproductivity and adaptability to a new environment. However, the limitation is that it highly depends on the accuracy of the original data. As shown in Fig. 1, if the original demonstration data are unreliable and different from the real one, there is also a risk that the estimated distribution will be outside the real one, leading to invalid robot motion. Hence, the target is limited to the motion in a less-cluttered environment when using image data as an original information resource.

Therefore, since these two existing frameworks have difficulty dealing with unreliable and limited number of demonstrations, technical breakthroughs for overcoming the limitation are required to achieve the purpose of this study.

B. Experience-Based Motion Planning

This study also depends on previous studies in other research fields: experience-based motion planning [21], [22], [23], [24], [25]. Similar to LfD, the planning problem is not solved in planning from scratch (PFS). Particularly, past planning problems (path experiences) results are used as a clue for solving new problems instead of using demonstration data. The main features of this methodology are its flexibility and robustness to changes in the surrounding environment. Because the environment in which the past solution was found is often different from the current one, it is difficult to directly transfer and reuse past planning results for a new problem. Hence, many of these studies have modified and deformed the path experience and explored unknown regions in robot configuration space (C-space) [23], [24], [25].

Among them, one of the state-of-the-art techniques in this area, i.e., the experience-driven random tree connect (ERTC) [25], has the high ability to compensate for the differences between the previous environment in which the path experience was found and the current one, and can deal with various planning problems with small numbers of experiences (less than 100). To fit small numbers of experiences to various environments, it decomposes the path experience into several micro-experiences and partially adds random morphing to a wider search in the joint configuration space (C-space) beyond the range of the reference path. This flexible deformation process can fix the violated part of the path experience caused by differences between the previous and current environments. Therefore, introducing the path adaptation function of ERTC into the LfD framework has a potential to solve the pre-mentioned problems of existing methodologies. However, no studies have been conducted on this aspect.

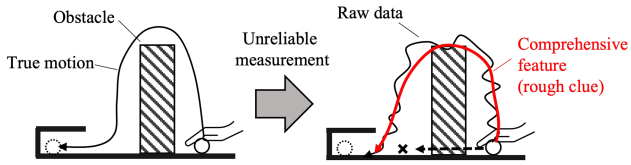

Fig. 2. Comprehensive feature of the human motion implicitly included in the unreliable demonstration data.

III. Methods

A. Overview of Proposed Method

Based on this background, this study aims to develop a new motion planning framework, named experience-driven random tree connect with human demonstration (ERTC-HD), which can facilitate the identification of valid robot motions in a cluttered environment by only using human skeletal information extracted from a single RGB camera image.

The main concept of ERTC-HD is to only extract the comprehensive feature of human motion from unreliable skeleton information and use it as a rough clue for solving difficult robot motion planning problems. As shown in Fig. 2, human motion data implicitly includes information about the surrounding environment, such as the shape and position of the obstacles, even if it includes a large amount of noise. Therefore, if we can extract and reflect it into the motion planning process, we expect that the motion planner will find the valid motion much faster than PFS, which uses such unreliable demonstrations. Also, since it only extracts one feature trajectory from tens to several tens of demonstrations, ERTC-HD can be applied to a small amount of data.

Fig. 3 shows the overall flow of the ERTC-HD. First, it tries to extract the comprehensive feature of the human motion data, modeling and generalizing it to the various problems (Fig. 3(a)–(c)). The extracted human motion is converted to the robot motion and saved into the motion database as a path experience for the ERTC planner (Fig. 3(d)–(e)). Finally, one of the selected path experiences is mapped and adjusted to the new environment. The invalid part is modified by the path decomposition and morphing process (Fig. 3(f)).

B. Contributions

There are several contributions to the proposed ERTC-HD framework. First, we achieved a significant reduction of the

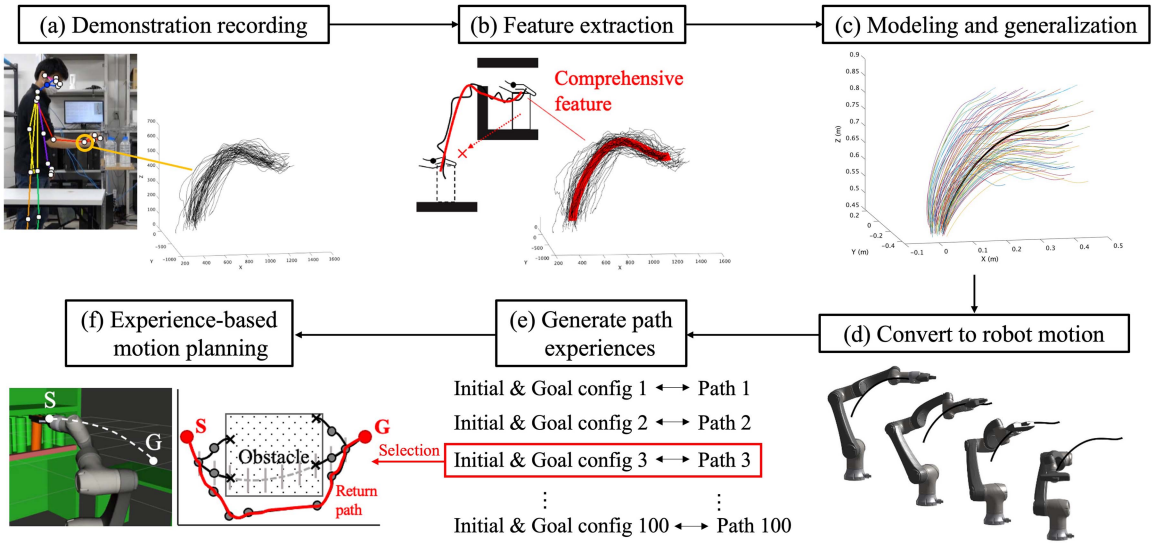

Fig. 3. Overall flow of proposed method ERTC-HD.

required accuracy of the original information resources for LfD planning by introducing our original processing flows (Fig. 3). Different from previous studies using detailed information of demonstrations (e.g., [16]), ERTC-HD only extracts and uses the comprehensive feature of the human demonstration; hence it only requires enough accuracy to catch up a rough feature of human motion, such as several to ten centimeters, as shown in later experiments. This can extend its application range from simple, easy planning problems [4], [5], [6], [7], [8] to more difficult and practical ones. Also, we first proposed the idea of developing the path experiences from human demonstrations. This allows us to make high-quality and stable experiences, and overcome the problem of variance of experiences generated from a random sampler [21], [22], [23], [24], [25]. Finally, through the simulation experiments, we confirmed the effect of the accuracy of demonstrations on LfD planners by comparing the results between using motion capture data ($\sim$1.0 mm) and RGB image data ($\sim$10 cm). This will clarify issues in current LfD studies and bring further development.

C. Problem Definition

The robot motion planning problem addressed in this study is defined as a mathematical problem of finding a collision-free path in a C-space $Q \in \mathbb{R}^n$, from a particular initial configuration $\boldsymbol{q_{ini}} \in Q$ to the goal configuration $\boldsymbol{q_{goal}} \in Q$. The dimension n of the C-space corresponds to the degree of freedom (DoF) of the robot; $n = 6$ for a standard industrial robot arm, including the one used in this study (Elfin 5 arm). The expression $Q_{obs} \subset Q$ indicates the space occupied by obstacles in the environment; its size increases with the number of obstacles in the environment. Hence, it is difficult to sample from valid (collision-free) spaces ($Q_{free} = Q \setminus Q_{obs}$) when the robot moves in a cluttered environment.

D. Steps of Proposed Method (ERTC-HD)

1) Data Measurement: In the process of ERTC-HD, first, the human demonstrator shows the ideal motion of the target task in front of a single RGB camera. This is repeated several to ten times for each task. The collected image sequence data is input to the skeleton recognition software, and it returns the 3-dimensional joint position information of the wrists and elbows of the right arm. Also, since pose information (roll, pitch, and yaw angle) of the hand are lacking, which is required for generating the robot motion, we estimated it from elbow and wrist position data by assuming two heuristics: 1) the tips of the hands tend to be located on a straight line connecting the elbow and wrist joints, and 2) twisting motions are not dominant in most human motions, except for some specific motions, such as opening the lid of a plastic bottle. From the former, we can estimate the pitch and yaw angles of the human hand; from the latter, we set the roll angle as a constant equal to 0.

2) Extracting Comprehensive Feature of the Human Motion: As a result of the former process, we obtain the required information for generating the robot motion. However, it is difficult to be directly converted to the robot motion due to the large amount of noise in the collected data, as shown in Fig. 3(a). Therefore, to address this issue, we designed original processing flows to extract the comprehensive feature of the human motion data from noisy demonstrations.

First, a low-pass filter was used for extracting the slow-changing components from the measured data. Here, we defined the "comprehensive feature" of human motion as the slow-changing components representing the outline of the human motion in the target tasks, such as "the human does not move their hand in the straightforward direction to avoid the obstacles in the environment" (Fig. 2). To extract such key information from a noisy motion data, a cutoff frequency of 1 Hz which is much lower than that of conventional biomechanics for human kinematics data (10–50 Hz [26]) was specifically applied. Then, the filtered data is averaged, and the feature trajectory is extracted (Fig. 3(b)). When taking the averaged filter to the different lengths of motion data, an interpolation technique is used and standardized to the N point data ($N = 101$ in this study). This alignment of the data length will stabilize the performance of the later ERTC process by consistent the length of micro-experience.

Fig. 4 shows an example of a 3-dimensional right wrist trajectory and the estimated pitch and yaw angle by comparing

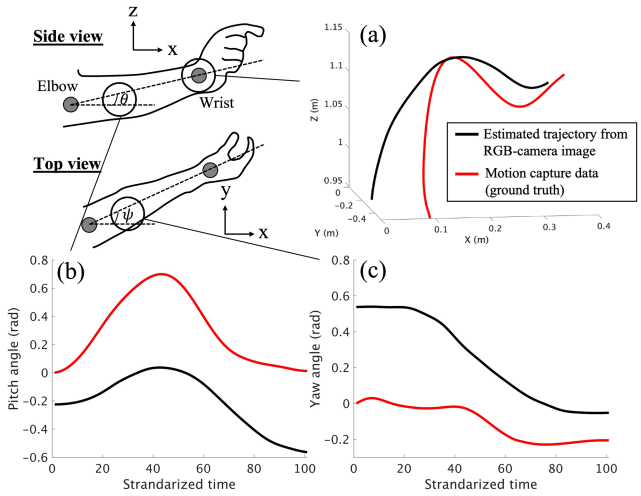

Fig. 4. Human hand position and pose information generated from the proposed method. The red line shows the motion capture data as the ground truth. This figure shows the data of experimental task 1 as an example (Fig. 7(a)).

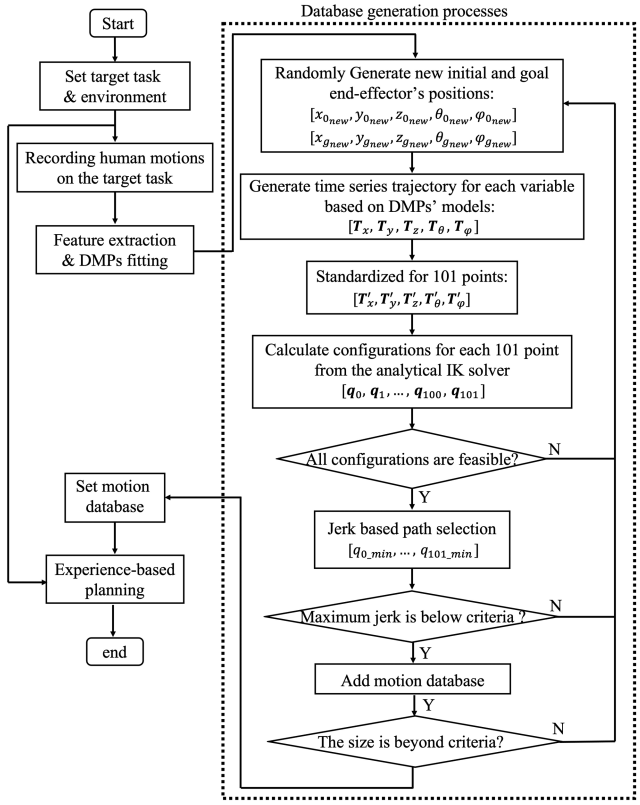

Fig. 5. Flowchart of generating robot motions and motion database from DMPs models (the parts surrounded by the dotted line) and its role in entire ERTC-HD processes.

the motion capture data as the ground truth. Although there is a certain amount of estimation error, the comprehensive features of human motion can be captured.

3) Modeling and Generalization: After extracting the features, it is modeled using the dynamic movement primitives (DMPs) model and generalized (Fig. 3(c)). The DMPs model is the representative technique for modeling the demonstration data. Since it can easily simulate obstacle-avoidant motion [27],

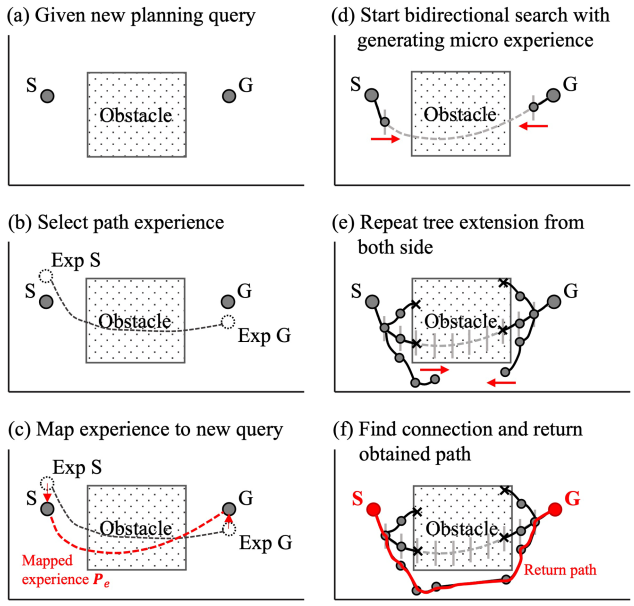

Fig. 6. Process of ERTC algorithm (adapted from [25]).

[28], we adopted it for the modeling part of the ERTC-HD. The point of this part is that by aggregating noisy demonstrations into one typical motion and then expanding and generalizing them again, we expect to generalize the limited number of noisy demonstration data while maintaining the characteristics of natural human motion.

Particularly, we adopt the DMPs model developed by Pastor et al. [28]. In their model, the time evolution of each variable is represented by the following equations:

$$\tau \dot{v} = K\left(g - x\right) - Dv - K\left(g - x_0\right)s + Kf\left(s\right) \quad (1)$$

$$\tau \dot{x} = v \quad (2)$$

where x is the one-dimensional time series of position or angle data of the human hand, and v represents the velocity of the parameter (e.g., hand velocity for x-direction), and $\dot{v}$ represent acceleration. Hence, the basic structure of the equation of (1) is the spring-mass-damper model, and $f(s)$ has the role of the external force to drive the model. x_0 and g represent the start and goal values. K and D are constants corresponding to the spring and damping terms and are set to 0.01 and 0.3 in this study. s is the phase variable and it represents the sequence of the motion which monotonically changes from 1 to 0 (0 represents the end of the motion). τ is the temporal scaling factor to control the number of data points, and set as 1.0. $f(s)$ is a non-linear function defined as:

$$f\ \left(s\right) = \frac{\sum_i w_i \psi_i\left(s\right) s}{\sum_i \psi_i\left(s\right)} \quad (3)$$

where $\psi(s)$ is the Gaussian basis function. Intuitively, $f(s)$ is calculated by overlaying multiple Gaussian distributions with different weights, and this represents the time-varying external forces to reproduce the dynamic interaction with the environment (e.g., getting a large pulse force when it closes to the obstacles). Hence, by fitting (3) to the human motion data, we can extract information about the surrounding environment from it. We set 10 Gaussian basis functions with its centers μ_i increments in 0.1 from 0.1 to 1, and variance σ_i are set as 1.0. The fitting of

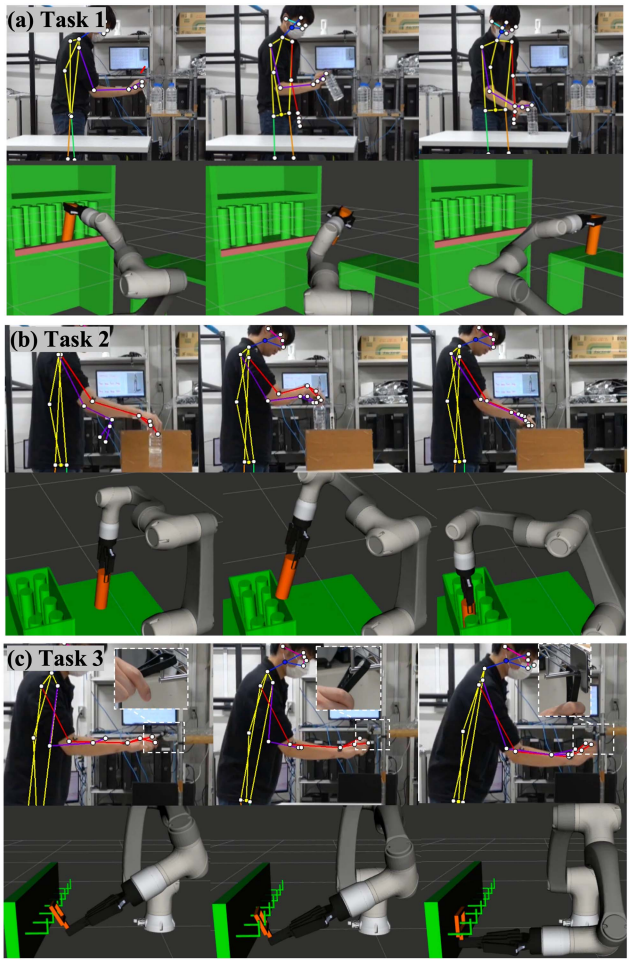

Fig. 7. Target tasks of simulation experiment; (a) picking object from the shelf, (b) placing object between obstacles, (c) hanging hollow object on the hook.

the DMPs model was separately done by adjusting the weight parameters w_i of (3) for each variable; hence, we developed five DMPs models.

4) Generating Robot Motion as Path Experience: Then, the robot motion is generated based on generalized motions in the former process (Fig. 3(d)) and saved in the motion database as the path experience for the ERTC planner (Fig. 3(e)). This part aims to increase the quality of the path database by generating the path experience from human demonstrations. This can address the issue of variations in path experiences due to using a random sampling method for generating experiences [21], [22], [23], [24], [25].

Regarding converting human motion to robot motion, this study adopted jerk-based mapping since it showed a high ability to reproduce natural human hand motion [29]. Fig. 5 shows the flowchart of the process and its role in the whole process. First, a pair of initial and goal positions and the pose of the end-effector were randomly assigned for each DMPs model. The values of these variables should be well-represented in the environment in which the robot moves. For example, in the case of experimental task 1 in this study (Fig. 7(a)), the mean values of the start and goal positions should be set at the center of the lined-up objects and above the center of the desk. Owing to the variation in the position of the lined-up objects, the goal positions of the end-effector should be varied more widely (e.g., $\pm$0.3 m) than the initial position (e.g., $\pm$0.03 m).

Then, the time series trajectory for each variable is generated based on each DMPs model. The obtained time series data are standardized for 101 points and set as the desired robot end-effector's position and pose (the roll angle is set to be constant (0 rad)). Next, by using an analytical inverse kinematic (IK) solver for a 6-DoF robotic arm, robot joint configurations for reproducing each of the 101 states were calculated. If all 101 points are feasible, the motion path is selected to minimize the total jerk from the initial position to the goal position in the C-space. The initial and end positions are re-assigned if the maximum jerk between each point in the trajectory is larger than the criterion (1.0 for this study) for keeping the quality of path experience. The process ends when the database size reaches the criterion (100 experiences for this study).

5) Experience-Based Planning With Motion Database: Finally, experience-based planning is performed by the ERTC planner. While the original ERTC planner used past results of random sampling planners as experience [25], this study used robot motion generated by human demonstration. This enables us to tell the knowledge of the surrounding environments implicitly included in the human motion to the planner and search more effectively in vast C-space.

Since we only extracted the comprehensive feature of the human motion, the violated part of the experience path is modified by the followed ERTC process. Fig. 6 shows a schematic of the process. First, when a new motion planning problem is given, the path experience $\boldsymbol{P}_e$ is selected based on the similarity of the initial configuration $\boldsymbol{q}_{ini\_new}$ and goal configuration $\boldsymbol{q}_{goal\_new}$ (Fig. 6(a)–(b)). Path experience is the motion trajectory in the C-space (time series of 6 joint angles of the 6-DOF robot), and it corresponds to the solution found in past planning problems. Then, the selected path experience $\boldsymbol{P}_e = [\boldsymbol{q}_{e_0} \cdots \boldsymbol{q}_{e_{101}}]^T$ is mapped to the new problem with an affine transformation (Fig. 6(c)):

$$\boldsymbol{P}_{map} = \boldsymbol{\lambda}_{n\times 101} \cdot \boldsymbol{P}_e + \boldsymbol{b}_{n\times 1} \tag{4}$$

where $\boldsymbol{b}_{n\times 1} = \boldsymbol{q}_{ini\_new} - \boldsymbol{q}_{e_0}$ is the shifting vector used to equalize the initial position; $\boldsymbol{\lambda}_{n\times 101} = [0\ \frac{\boldsymbol{\alpha}}{100}\ \frac{2\boldsymbol{\alpha}}{100} \cdots \boldsymbol{\alpha}]$ with $\boldsymbol{\alpha} = \frac{\boldsymbol{q}_{goal\_new} - \boldsymbol{b}_{n\times 1}}{\boldsymbol{q}_{e_{101}}}$ is the shear coefficient to equalize the goal position. The dimensions of these parameters and search space n was set as 6 for the 6-DoF robotic arm used in this study.

Then, we start the bidirectional search (Fig. 6(d)). First, one node in the start or goal tree is selected; a micro experience is generated from it by adding a random affine transformation, as in (4), and tries to extend to a new space and connect to the other tree. Through the iteration of this tree extension process, it can search for a wider range beyond the range of the original experience (Fig. 6(e)). The length of the micro experiences generated from the selected node is varied for each iteration and is the hyperparameter of this algorithm. We set the default values (5% - 10% for total length) from the study in [25]. Finally, if a valid connection between two trees is found, the obtained path is returned (Fig. 6(f)).

IV. Experiments

A. Overview

A simulation experiment was performed to verify the performance of the proposed method by comparing it with state-of-the-art planners. Regarding benchmark tests for the motion planner [30], three difficult planning problems with different tasks in the cluttered environment were selected, as shown in Fig. 6. The task in Experiment 1 was to pick up a specific lined-up object from the shelf (Fig. 7(a)). In this task, both humans and robots need to tilt the object toward the front direction (to their body) and move it diagonally upwards to avoid collisions with obstacles. Additionally, the task in Experiment 2 was to place the object between the obstacles in the box (Fig. 7(b)). In this task, the object is moved straight down while maintaining its pose during the placing (latter) phase. Finally, in Experiment 3, the robot and human tried to hang hollow objects on the hook (Fig. 7(c)). This is expected to be a particularly difficult planning problem because it strictly constrains the position and pose of the end-effector.

In addition, to verify the robustness to the unreliability of the demonstration data and changes in the surrounding environment, two experimental conditions were set. The first one was to use a single RGB camera image with human skeleton tracking software to measure the human demonstration; the environment in which the robot engaged in the task was randomly changed and was inconsistent with the actual working environment (Condition 1). The other condition was to use a motion capture camera for data collection and set a consistent environment with the actual one (Condition 2). Hence, the accuracy and reliability of the demonstration data were higher in the latter condition than in the former one. Therefore, it is expected that if the performance of the planner depends on the reliability of the demonstration data, the success rate of the planning will decrease and take a longer calculation time when using a single RGB camera image as an information resource.

B. Experimental Setup

1) Measurement of Human Demonstration Data: To measure the demonstration data, a human demonstrator repeatedly performed the target task in front of a single RGB camera (SONY, FDR-AX45A, 60 fps) and 10 motion capture cameras (NAC image technology, Kestrel2200, 100 Hz). For measurements with the motion capture system, the human hand pose was directly measured from the right wrist, palm, index finger, and thumb position data. The calibration results of the motion capture camera system showed that the accuracy of the position data was ± 0.47 mm. The total number of measurement data was 60 for task 1 (6 lined-up objects and 10 times iterations), 80 for task 2 (8 placement positions and 10 iterations), and 70 for task 3 (7 target positions and 10 iterations).

The images obtained from the RGB camera were analyzed using human skeleton tracking software (NEXT-SYSTEM, VisionPose), and three-dimensional human skeleton information was extracted. The x-, y-, and z-axes were defined as the direction of the vector perpendicular to the frontal, sagittal, and transverse planes of the human body at the start time of the task. The comparison between the right wrist trajectory during the tasks generated from the process of the proposed method and motion capture data as a ground truth showed that the mean estimation errors from the RGB camera images were ± 4.5 cm, ± 15.4 cm, ± 2.4 cm, and ± 0.051 (rad), ± 0.038 (rad), for x, y, and z directional position data, respectively, and pitch and yaw angle data, respectively. The position data of the equipment, such as the corners of the shelf and desk, were also measured by a motion capture system for constructing the corresponding simulation environment.

2) Construction of Simulation Environment: Based on the motion capture data of the working environment, the simulation environment for Condition 2 was reproduced, including six motion planning problems (corresponding to the number of lined-up objects) set for task 1, eight motion planning problems (number of placing positions inside the box) set for task 2, and seven motion planning problems (number of hooks) set for task 3 in. These correspond to the robot attempting to perform the same task in the same environment.

Additionally, to verify the capability of the planner to cope with the variability of the environment, variations were added to the environment of each task for Condition 1. In task 1, the position of the shelf was randomly varied within the range of ± 0.30 m for each axis, and the target object picked up from the shelf was also randomly changed within the six lined-up objects in the front row. In task 2, the position of the table with the box was randomly varied within the range of ± 0.30 m for each axis, and the placement position was also randomly changed among the eight candidates. Finally, in task 3, the position of the wall with seven hooks was randomly varied within the range of ± 0.30 m for each axis, and the target hook was randomly selected. A total of 100 problems were randomly generated for each experimental task under Condition 1.

3) Planner Implementation: Four motion planners were implemented and used to solve the planning problem for each experimental task and condition, i.e., ERTC-HD, ERTC-RRTC, GMR-RRT, and RRTC. ERTC-HD is the proposed method of this study and is implemented by the process mentioned in the previous sections. ERTC-RRTC is a state-of-the-art experience-based motion planner developed by Pairet et al. [25]. The difference from the proposed method is how the path experience is generated. This method uses the RRTC algorithm in a simplified environment to remove obstacles. GMR-RRT is a state-of-the-art model-based LfD motion planner [20], which generates a GMR model from the demonstration data and adds a bias to the sampling regions of the RRT sampler. As in the study in [20], the ratio of biased sampling to random sampling was set to be 1:1 to ensure the generalizability of the algorithm. Notably, while the original GMR-RRT$*$ algorithm performs RRT$*$ sampling after the solution is found to guarantee optimality, only the part that searches for an initial solution was used in this study. Hence, we used the term GMR-RRT instead of GMR-RRT$*$. Finally, for comparison with the motion planner that adopts the PFS strategy, we also implemented the RRTC.

For preparing the path experience for ERTC-HD, a total of 100 experiences were generated based on the human skeleton information (Condition 1) and motion capture data (Condition 2) by adding the same range of variance of initial and goal positions in the DMPs model (i.e., ± 0.30 m for each axis). The same number of path experiences was randomly generated for the ERTC-RRTC by solving the simplified problem with the RRTC planner same as the original study [25]. The simplification of each planning problem is achieved by removing the lined-up object from the environment (i.e., only the existing shelf and table) for task 1, the objects within the box for task 2 (i.e., only the existing box and table), and a part of the hook (front,

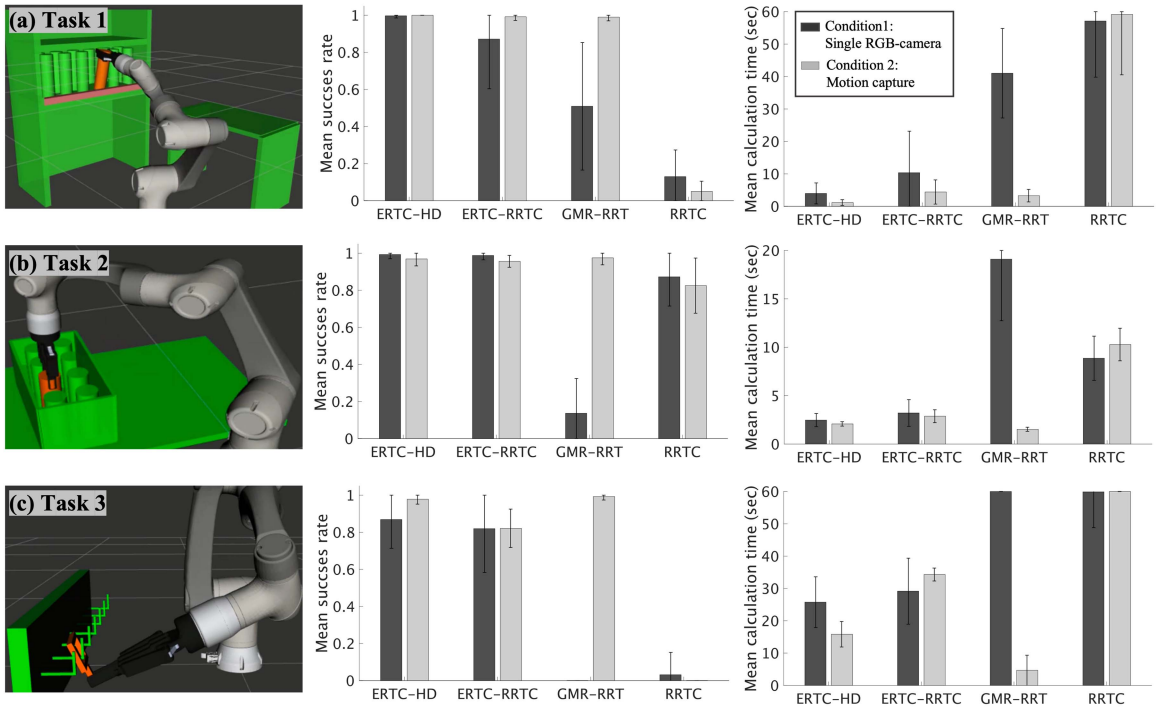

Fig. 8. Results of simulation experiments: Mean success rate (middle column) and mean calculation time (right column) for each experimental task (task 1: Upper row, task 2: Middle row, task 3: Lower row) and condition (condition 1: Black bar, condition 2: Gray bar). The error bar represents the standard deviation.

vertical extended part) for task 3. The environmental variation was also added within the same range of ERTC-HD. The GMR model for GMR-RRT was generated based on the same 100 path experiences as those of ERTC-HD.

The simulation ran on an Intel i5 Linux machine with 2.0 GHz cores and 16.0 GB RAM. The Robot Operating System (ROS) with Open Motion Planning Library (OMPL) was used to develop the simulation environment and implement the motion planners. Each problem was solved 20 times by setting the limitation time to 60, 20, and 60 s for each task while considering their difficulty. The planners were evaluated based on the mean success rate and mean calculation time.

D. Results and Discussions

Fig. 8 shows the results of the simulation experiments. As shown in Fig. 8, the proposed method ERTC-HD showed the highest performance in each experimental task. By comparing the results of GMR-RRT, a state-of-the-art LfD planner, although GMR-RRT showed a significant decrease in success rate when using human skeletal data (99% to 51% for task 1, 98% to 14% for task 2, 99% to 0% for task 3), ERTC-HD can solve difficult problems within shorter time, even when using unreliable skeleton data (99% with 3.9 s for task 1, 99% with 2.5 s for task 2, and 87% with 25.7 s for task 3). Therefore, while the performance of a conventional LfD planner highly depends on the accuracy of the original demonstration data, the proposed framework can facilitate the planning even by using unreliable demonstrations. This trend is more obvious following increased task difficulty (task 3). Also, the reason for GMR-RRT showed better performance in task 1 than task 2 may be due to the differences in limitation of the time (60 sec for task 1 and 20 sec for task 1) or the estimation accuracy of the human skeleton is worse in task 2 due to the occlusion of the box (Fig. 7(b)).

In addition, the proposed method also showed higher performance than ERTC-RRTC. Using the path experience generated from human skeleton information via a single RGB camera (Condition 1) can significantly reduce the calculation time compared to using the results of RRTConnect (76% reduction for task 1, 76% reduction for task 2, and 11% reduction for task 3). These results suggest that human demonstration is more informative than the results of random sampling-based planners, even if it is measured by a single vision sensor. Although ERTC-RRTC showed robustness for variation of the environment (condition1) as shown in the previous study [25], our method can obtain a valid solution quicker by using a path experience generated from human demonstration data, and this is more evident when using more precious human information collected by motion capture system (condition 2).

Finally, by comparing the results of the PFS planner (RRTC), the proposed method can significantly increase the success rate of the planning and decrease the computation time by using a single RGB camera image (93% reduction for task 1, 22% for task 2, and 56% for task 3). RRTC almost failed in planning and showed the worst performance in tasks 1 and 3. However, it performed better in task 2 of condition 1 for GMR-RRT. This suggests that the unreliable demonstration sometimes makes the performance of the LfD planner worse than a random sampling method. Therefore, to deal with unreliable information resources, it would be better not to use it directly as a solution for planning but as a rough clue for finding the valid regions in C-space.

V. Conclusion and Future Work

In conclusion, the proposed motion planning framework of this study, ERTC-HD, can facilitate the identification of valid motions in a cluttered environment using unreliable human

skeletal information extracted from single RGB camera images. The results of simulation experiments showed higher performance than the state-of-the-art motion planners owing to its less-strict usage of the demonstration data, especially in the case of using unreliable human skeleton information as demonstration data. Specifically, the proposed method can significantly increase the success rate and reduce calculation time by 57%–98% compared to the state-of-the-art LfD planner and 11%–76% for the state-of-the-art experience-based planner.

Finally, there are several limitations in this study. First, because the proposed method can only estimate the yaw and pitch angles of the human hand owing to the limited number of joints that the skeleton tracking software can detect, the roll angle should also be detected in the future by combining a 3-dimensional pose estimation technique of the hand or objects. Moreover, as our proposed method cannot ensure the optimality of the planning path, we will improve it to guarantee the optimality. Finally, we only performed simulation experiments, and our findings need to be verified with actual robots in real-world situations in the future.

ACKNOWLEDGMENT

This letter is one of the achievements of joint research with and is jointly owned copyrighted material of ROBOT Industrial Basic Technology Collaborative Innovation Partnership.

REFERENCES

[1] Z. Xie, Q. Zhang, Z. Jiang, and H. Liu, "Robot learning from demonstration for path planning: A review," *Sci. China Technol. Sci.*, vol. 63, no. 8, pp. 1325–1334, 2020.

[2] L. Song, G. Yu, J. Yuan, and Z. Liu, "Human pose estimation and its application to action recognition: A survey," *J. Vis. Commun. Image Representation*, vol. 76, 2021, Art. no. 103055.

[3] H. Ravichandar, A. S. Polydoros, S. Chernova, and A. Billard, "Recent advances in robot learning from demonstration," *Annu. Rev. Control, Robot., Auton. Syst.*, vol. 3, pp. 297–330, 2020.

[4] C.-Y. Liu, J.-J. Liang, T.-H. S. Li, and K.-C. Chang, "Motion imitation and augmentation system for a six degrees of freedom dual-arm robot," *IEEE Access*, vol. 7, pp. 153986–153998, 2019.

[5] D. A. Duque, F. A. Prieto, and J. G. Hoyos, "Trajectory generation for robotic assembly operations using learning by demonstration," *Robot. Comput.-Integr. Manuf.*, vol. 57, pp. 292–302, 2019.

[6] J. Li, J. Wang, S. Wang, and C. Yang, "Human-robot skill transmission for mobile robot via learning by demonstration," *Neural Comput. Appl.*, vol. 33, pp. 1–11, 2021.

[7] M. Dagioglou, A. C. Tsitos, A. Smarnakis, and V. Karkaletsis, "Smoothing of human movements recorded by a single RGB-D camera for robot demonstrations," in *Proc. 14th PErvasive Technol. Related Assistive Environ. Conf.*, 2021, pp. 496–501.

[8] K. Wang, Y. Fan, and I. Sakuma, "Robot programming from a single demonstration for high precision industrial insertion," *Sensors*, vol. 23, no. 5, 2023, Art. no. 2514.

[9] Y. Chen, Y. Tian, and M. He, "Monocular human pose estimation: A survey of deep learning-based methods," *Comput. Vis. Image Understanding*, vol. 192, 2020, Art. no. 102897.

[10] G. Gulletta, W. Erlhagen, and E. Bicho, "Human-like arm motion generation: A review," *Robotics*, vol. 9, no. 4, 2020, Art. no. 102.

[11] C. Zhang, S. Bengio, M. Hardt, B. Recht, and O. Vinyals, "Understanding deep learning (still) requires rethinking generalization," *Commun. Assoc. Comput. Machinery*, vol. 64, no. 3, pp. 107–115, 2021.

[12] M. Simonič, T. Petrič, A. Ude, and B. Nemec, "Analysis of methods for incremental policy refinement by kinesthetic guidance," *J. Intell. Robot. Syst.*, vol. 102, 2021, Art. no. 5.

[13] T. Brys, A. Harutyunyan, H. B. Suay, S. Chernova, M. E. Taylor, and A. Nowé, "Reinforcement learning from demonstration through shaping," in *24th Int. Joint Conf. Artif. Intell.*, 2015, pp. 3352–3358.

[14] K. Pertsch, Y. Lee, Y. Wu, and J. J. Lim, "Guided reinforcement learning with learned skills," in *Proc. Conf. Robot Learn.*, 2021, pp. 729–739.

[15] Y. Qin, H. Su, and X. Wang, "From one hand to multiple hands: Imitation learning for dexterous manipulation from single-camera teleoperation," *IEEE Robot. Automat. Lett.*, vol. 7, no. 4, pp. 10873–10881, Oct. 2022.

[16] S. P. Arunachalam, S. Silwal, B. Evans, and L. Pinto, "Dexterous imitation made easy: A learning-based framework for efficient dexterous manipulation," in *Proc. IEEE Int. Conf. Robot. Automat.*, 2022, pp. 5954–5961.

[17] Y. H. Wu, J. Wang, and X. Wang, "Learning generalizable dexterous manipulation from human grasp affordance," in *Proc. Conf. Robot Learn.*, 2023, pp. 618–629.

[18] B. Akgun, M. Cakmak, K. Jiang, and A. L. Thomaz, "Keyframe-based learning from demonstration: Method and evaluation," *Int. J. Social Robot.*, vol. 4, pp. 343–355, 2012.

[19] A. Pervez, A. Ali, J.-H. Ryu, and D. Lee, "Novel learning from demonstration approach for repetitive teleoperation tasks," in *Proc. IEEE World Haptics Conf.*, 2017, pp. 60–65.

[20] J. Wang, T. Li, B. Li, and M. Q.-H. Meng, "GMR-RRT∗: Sampling-based path planning using Gaussian mixture regression," *IEEE Trans. Intell. Veh.*, vol. 7, no. 3, pp. 690–700, Sep. 2022.

[21] M. Phillips, B. Cohen, S. Chitta, and M. Likhachev, "E-graphs: Bootstrapping planning with experience graphs," in *Proc. Int Symp. Combinatorial Search*, 2012, vol. 3, pp. 188–189.

[22] D. Berenson, P. Abbeel, and K. Goldberg, "A robot path planning framework that learns from experience," in *Proc. IEEE Int. Conf. Robot. Automat.*, 2012, pp. 3671–3678.

[23] D. Coleman, I. A. Şucan, M. Moll, K. Okada, and N. Correll, "Experience-based planning with sparse roadmap spanners," in *Proc. IEEE Int. Conf. Robot. Automat.*, 2015, pp. 900–905.

[24] C. Chamzas, A. Shrivastava, and L. E. Kavraki, "Using local experiences for global motion planning," in *Proc. Int. Conf. Robot. Automat.*, 2019, pp. 8606–8612.

[25] È. Pairet, C. Chamzas, Y. Petillot, and L. E. Kavraki, "Path planning for manipulation using experience-driven random trees," *IEEE Robot. Automat. Lett.*, vol. 6, no. 2, pp. 3295–3302, Apr. 2021.

[26] E. Kristianslund, T. Krosshaug, and A. J. Van den Bogertm, "Effect of low pass filtering on joint moments from inverse dynamics: Implications for injury prevention," *J. Biomech.*, vol. 45, no. 4, pp. 666–671, 2012.

[27] D.-H. Park, H. Hoffmann, P. Pastor, and S. Schaal, "Movement reproduction and obstacle avoidance with dynamic movement primitives and potential fields," in *Proc. IEEE-Robot. Humanoids 8th Automat. Soc. Int. Conf. Humanoid Robots*, 2008, pp. 91–98.

[28] P. Pastor, H. Hoffmann, T. Asfour, and S. Schaal, "Learning and generalization of motor skills by learning from demonstration," in *Proc. IEEE Int. Conf. Robot. Automat.*, 2009, pp. 763–768.

[29] U. Pattacini, F. Nori, L. Natale, G. Metta, and G. Sandini, "An experimental evaluation of a novel minimum-jerk Cartesian controller for humanoid robots," in *Proc. IEEE/RSJ Int. Conf. Intell. Robots Syst.*, 2010, pp. 1668–1674.

[30] C. Chamzas et al., "MotionBenchMaker: A tool to generate and benchmark motion planning datasets," *IEEE Robot. Automat. Lett.*, vol. 7, no. 2, pp. 882–889, Apr. 2022.